New Journal of Physics
The open access journal at the forefront of physics

Deutsche Physikalische Gesellschaft DPG IOP Institute of Physics

PAPER • OPEN ACCESS

Fabrication of $^{15}NV^-$ centers in diamond using a deterministic single ion implanter

To cite this article: Karin Groot-Berning *et al* 2021 *New J. Phys.* **23** 063067

New Journal of Physics
The open access journal at the forefront of physics

Deutsche Physikalische Gesellschaft DPG
IOP Institute of Physics

Published in partnership with: Deutsche Physikalische Gesellschaft and the Institute of Physics

OPEN ACCESS

RECEIVED
6 January 2021

REVISED
18 May 2021

ACCEPTED FOR PUBLICATION
2 June 2021

PUBLISHED
23 June 2021

PAPER

Fabrication of $^{15}NV^-$ centers in diamond using a deterministic single ion implanter

Karin Groot-Berning[1,*], Georg Jacob[2], Christian Osterkamp[3], Fedor Jelezko[3] and Ferdinand Schmidt-Kaler[1,4]

[1] QUANTUM, Johannes Gutenberg-Universität Mainz, Staudinger Weg 7, 55128 Mainz, Germany
[2] Alpine Quantum Technologies GmbH, Technikerstrasse 17/1, 6020 Innsbruck, Austria
[3] Institut für Quantenoptik, Universität Ulm, Albert Einstein Allee 11, 89081 Ulm, Germany
[4] Helmholtz-Institut Mainz, 55128 Mainz, Germany
[*] Author to whom any correspondence should be addressed.

E-mail: karin.groot-berning@uni-mainz.de

Keywords: deterministic implantation, single ion implantation, NV creation

Abstract

Nitrogen vacancy (NV) centers in diamond are a platform for several important quantum technologies, including sensing, communication and elementary quantum processors. In this letter we demonstrate the creation of NV centers by implantation using a deterministic single ion source. For this we sympathetically laser-cool single $^{15}N_2^+$ molecular ions in a Paul trap and extract them at an energy of 5.9 keV. Subsequently the ions are focused with a lateral resolution of 121(35) nm and are implanted into a diamond substrate without any spatial filtering by apertures or masks. After high-temperature annealing, we detect the NV centers in a confocal microscope and determine a conversion efficiency of about 0.6%. The ^{15}NV centers are characterized by optically detected magnetic resonance on the hyperfine transition and coherence time.

1. Introduction

1.1. Motivation

In the past two decades research on single nitrogen vacancy (NV) centers in diamond has undergone a dramatic progress. Since the first observation of single NVs with a confocal microscope and the demonstration of optically detected magnetic resonance (ODMR) [1], there have been numerous experiments which show a multitude of applications covering many fields such as metrology and quantum information processing. Among these applications are quantum sensors for magnetic and electric fields on the nanometer length-scale as well as microwave sensors [2].

A well established method to create NV centers is the implantation of nitrogen ions with subsequent annealing of the sample [3]. This approach is especially beneficial in cases where a precise placement of NVs is necessary. Typically, these are applications where the NVs are placed within dedicated structures in order to couple them to light fields e.g. inside a photonic waveguide structure [4, 5] or a solid immersion lens [6]. In these applications, implantation allows for circumventing the necessity of manufacturing such structures around pre-existing NV centers. The requirements on the resolution thereby, is given by the wavelength of the optical fields and thus is in the order of less than 100 nm. To this date, various techniques have been proposed and developed to reach that aim. For example, nanofabricated masks or pierced AFM tip which provide apertures [7, 8]. Another approach is using a focused ion beam with the respective resolution. This circumvents the need for employing a mask or an AFM tip near the focal plane [5]. However, these techniques are using stochastic sources, limiting the applications to cases where single NV devices can be post selected depending on whether an ion was implanted or not. This rules out applications which rely on coupling NV centers via their mutual dipolar magnetic interaction which is on the scale of a few tens of nanometers. Such a coupling between two NVs has been demonstrated in various experiments [9–11]. Scalable use of this resource e.g. for creation of entanglement in the context quantum information

processing calls for deterministic placement of single NVs with nanometer resolution. The need for arrays of single NVs at nanometer accuracy is even more important in view of building a scaled-up quantum processor or simulator based on this solid state platform [12–14].

To this goal we implement an intrinsically deterministic ion source by repetitively loading a single laser-cooled nitrogen molecular ion into a linear Paul trap and launch it from there. The laser cooling provides a small phase space occupation of the generated beam in both, the transversal and longitudinal direction. The former allows for tight focusing without need for spacial filtering which would destroy the deterministic property of the source. The latter results in a low energy dispersion, important for avoiding chromatic aberration when focusing by electric field lenses. Additionally, our method uses singly charged ions at energies lower than 10 keV, unlike methods that rely on the detection of single ion impact events [15]. The low energy implantation reduces position uncertainty due to straggling and surface destruction of the bulk diamond. Likewise the very same apparatus allows for transmission imaging of the substrate using single extracted calcium ions [16]. This provides a precise referencing and positioning of the dopants with respect to transmissive markers, free of parallax errors. Minimal charging and irradiation of the diamond substrate is ensured by using single ions for imaging. In this paper we present a proof of principle experiment which demonstrates the creation of NV centers with high resolution by focusing a nitrogen beam generated by this source. Although the deterministic production of single NV centers with this method is currently severely limited by the creation yield, additional measures—such as co-implantation of sulfur [17], surface termination [18], diamond overgrowth [19] and electron irradiation [20]—could realize such a truly deterministic creation process in the future. Also, the apparatus can be used as a deterministic source of any atomic and molecular ions and we envision for the future co-implanting of other ion species, e.g. $^{13}C^+$ ions, to tailor the spin-environment of the NV center.

2. Experimental apparatus and procedures

A linear Paul trap acts as an ultracold ion source [21–24]. The trap consists of four gold coated alumina chips mounted in an X-shaped arrangement, see reference [21] and figure 1 for details. One pair of diagonally opposing chips are supplied with RF voltage giving rise to a radial confinement of the ions. The chips of the other pair is segmented into 11 electrodes. These segments allow for shaping the axial potential by applying DC voltages. Along the axial direction, the trap is encapsulated by two pierced end-caps with a length of 10 mm, allowing for the extraction of the ions by switching them to high voltage.

Calcium atoms are provided by an oven which is directed towards the center of the trap. Inside the trapping volume the atoms are photo-ionized, trapped and laser cooled with light at 397 nm on the $S_{1/2}$ to $P_{1/2}$ dipole transition. Trapped ions are detected and automatically counted by imaging their fluorescence onto an EMCCD-camera[5]. The loading of a predefined number of calcium ions is accomplished by an automated procedure: first, a random number of ions is trapped, cooled and counted from the camera image. If necessary, ions are removed by lowering the axial trapping potential with a predefined voltage sequence. Subsequently, the success of this sequence is evaluated by counting the number of ions again and in case of discrepancy, the procedure is repeated.

Ion species other than calcium are loaded by means of a commercial ion gun[6] from gaseous sources as well as solid sources. The remainder of this paper is solely concerned with making use of the gaseous source. If the reader is interested in single-ions-on-demand from solid sources we refer to examples for praseodymium and thorium [21, 25]. We control the flux from the isotopically pure $^{15}N_2$ gas source[7] into the ion gun volume with a needle valve. Here, the molecules are ionized by electron impact. Subsequently the ions are extracted with typically 500 eV and are collimated to a beam which is guided and focused onto the hole of one of the trap endcaps. Deflection electrodes allow for blanking of this beam i.e. switching the loading of the trap on and off. For the gaseous source it is sufficient to direct the ion beam into the trap for a fixed period of time. Within an average loading time of about 30 s we are trapping one $^{15}N_2$ ion. We conjecture a loading mechanism facilitated by the modulation of the axial trapping potential due to the RF drive. This allows ions to enter the trap at the lower turning point of the axial potential modulation and keep them confined sufficiently long for sympathetic cooling such that their energy is reduced below the trap depth.

Note, that N_2^+ ions from the gas source enter the trap at random times which makes a successful capture more difficult, as compared to the case of laser-ablated targets where ions enter with a fixed time delay such that a time-dependent voltage sequence at the endcap electrodes can be employed to decelerate and capture

[5] Andor iXon X3, *DU-860E-CS0-UVB*, Andor Technology, Belfast, Northern Ireland.
[6] Ion Source *IQE 12/38*, SPECS Surface Nano Analysis GmbH, 13355 Berlin, Germany.
[7] Gas source $^{15}N_2$, 364584-1L-EU, 98% 15N, Sigma-Aldrich.

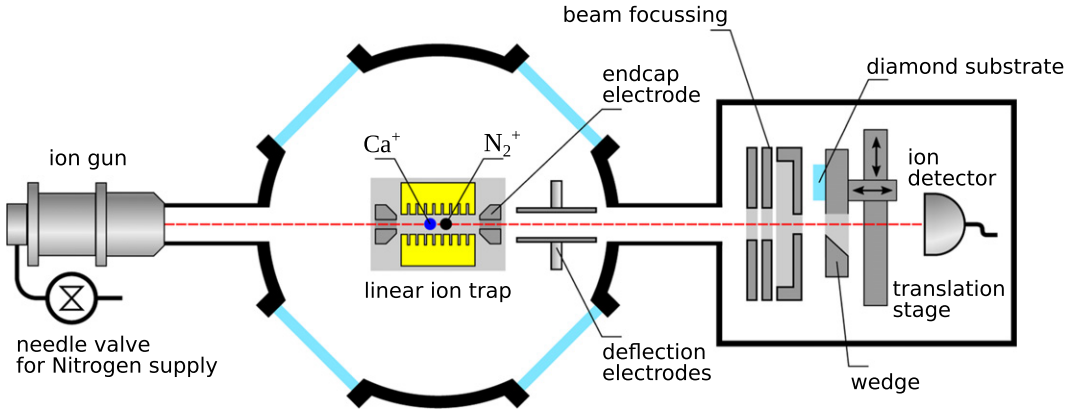

Figure 1. Sketch of the experimental setup: the ion gun serves as a source for molecular $^{15}N_2^+$ ions, which are loaded into the linear Paul trap together with atomic Ca^+ ions from an oven. A Wien filter after the ion gun (not shown) may be used. The ion extraction from the Paul trap is achieved by applying a voltage pulse to a pierced endcap electrode. A pair of deflection electrodes are used for beam steering, and the beam is focused with an Einzel-lens. A three-dimensional nano-translation stage with the probe holder and an optional wedged blade can be used for ion beam characterization together with the ion detector.

them [21]. Another challenge is the much higher gas load from the ion source towards the trap chamber, which we solve by differential pumping.

The nitrogen molecular ions are sympathetically cooled via their Coulomb interaction with the laser cooled calcium ions. A voltage sequence, similar to the aforementioned sequence for the loading of a given number of calcium ions, is applied in order to prepare a crystal consisting of exactly one calcium and one nitrogen molecular ion. The existence of a trapped nitrogen ion is detected by a shift of the calcium ion from its former equilibrium position on the camera image to the side, whereas the other ion does not emit light, thus coined briefly '*dark ion*'.

The deterministic source is implemented by extracting the single ion(s) from the trap. The accelerating electric field is provided by applying high voltages of up to -3 kV to one of the pierced endcaps. The ion kinetic energy is doubled by switching the voltage to a positive value while the ion is inside the endcap hole. Alignment and scanning of the ion beam is accomplished by two pairs of deflection electrodes which are placed along the ion pathway. Depending on the charge to mass ratio, the dark ion is either faster or slower than the calcium ion. This fact can be harnessed to separate the calcium. In case of a higher charge to mass ratio compared to calcium, the dark ion e.g. $^{15}N_2$ will arrive earlier at the endcap. At the moment the dark ion is inside the endcap, the voltage of the endcap is switched to a positive value, deflecting the calcium ion back when approaching the endcap. In the case where the charge to mass ratio is lower, the dark ion will leave the endcap later than the calcium ion. Switching the voltage of the endcap to a positive value is performed when the calcium ion has already left the endcap, resulting in a lower energy compared to the dark ion. Because of this, the deflection electrodes act differently on the two ion species, resulting in a separation of the calcium ion.

For an unambiguous determination of the dark ion species, i.e. to identify the trapped particle as a successfully loaded $^{15}N_2^+$ molecular ion, we extract the ions and detect them after a flight of 428 mm in length using a secondary electron multiplier (SEM). The SEM is located at the very end of the beam-path and can be operated for ion detection if the target mount is moved out of the beam-path via a piezo translation stage (see figure 1). The overall detection efficiency was measured to be $96\% \pm 2\%$.

During ion extraction, we switch off the RF amplitude, to avoid shot-to-shot modifications of the ion trajectory. These modifications originate from the time dependent electric fields of the RF drive at the vicinity of the endcap in combination with a timing jitter of the exact onset of the extraction voltage. We determine the mass of the extracted ions, from time-of-flight (TOF) measurements, discriminating between $^{15}N_2^+$, $^{15}N^{14}N^+$, and $^{14}N_2^+$, see figure 2(a). The trigger for the HV switching and RF switching is chosen such that the velocity modification is minimal, see figure 2(b). Prior to extraction, we arrange the order of the ions in the linear crystal, such that the lighter nitrogen ion is ahead. This prevents a Coulomb interaction of the nitrogen ion with the heavier and thus slower calcium ion. The ordering of ions is achieved by briefly melting and then recrystallizing the crystal, followed by a check of the right ion order from an EMCCD image of the fluorescence. In future, we may apply deterministic and fast swapping, as demonstrated experimentally [26]. We focus the ion beam by an electrostatic lens, see [16] for details. To optimize and finally characterize the spot size, we sweep a mechanical wedge into the focus and find $\sigma_{Ca} = 11(2)$ nm, and $\sigma_{N2} = 121(35)$ nm, respectively, see figures 2(c) and (d). For this experiment the same

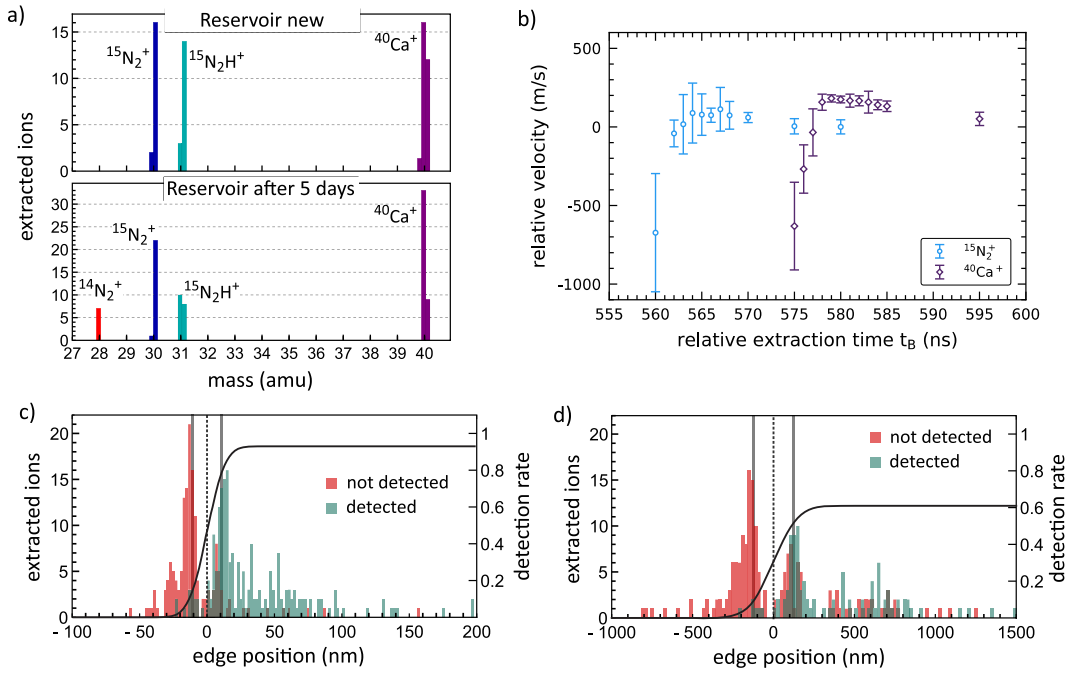

Figure 2. Ion beam characterization: we employ the SEM detector and remove the diamond sample from the ion pathway. (a) TOF signal in the SEM from single $^{15}N_2^+$, $^{15}N^{14}N^+$, and $^{14}N_2^+$, ions after a 0.428 m travel. After carefully purging all tube connections between $^{15}N_2$ gas bottle and ion gun we found no indication for $^{14}N_2^+$ ions. However, after a waiting time of 5 days, the histogram shows a peak at mass 28, which was assigned to the isotope ^{14}N. (b) Velocity variations of ^{40}Ca (diamond) and $^{15}N_2$ (dots) ions as a function of delay between RF and DC switching. Ions with a mass of 40 and 30, respectively, arrive at different times at the position of the endcap hole, and explore different phases of the RF drive field. (c) Focus spot determination of Ca ions, measured by sweeping the wedge into the beam and observing the partial blocking, which is detected from the SEM counts. For $^{40}Ca^+$ ions we obtain a $\sigma = 11(2)$ nm in x-direction. The data acquisition time for the extraction of 380 ions was approximately 17 min, which corresponds to a loading rate of 22.4 ions/min. (d) Focus spot determination of nitrogen molecular ions yielding $\sigma = 121(35)$ nm in x-direction. The measuring time for the extraction of 289 nitrogen ions takes about 117 min, which results in a loading rate of 2.5 ions/min. We conjecture thermal and electrical drifts as well as mechanical vibrations as major source of beam pointing fluctuations.

detector is used as for the TOF measurements. Note that the wedge positions for each shot was obtained using the Bayes experimental design method [27]. This leads to an accumulation of the positions around the turning points of the Gaussian error function, which was fitted to the data to obtain the sigma of the beam focus. We conjecture that long term drifts are affecting the spot size of the N_2^+, as the data acquisition time for the Ca^+ spot measurement is about 2 orders of magnitude faster. Sympathetic cooling of a dark ion of mass $u = 30$ with $^{40}Ca^+$ is expected to work efficiently, since the masses are about equal in the mixed crystal and thus the coupling of radial vibrational degrees of motion is still sufficient [28].

3. Sample preparation and implantation

Before any implantation was performed, the diamond host sample, a commercial type IIa electronic grade diamond from supplier Element Six, was investigated with a home-built confocal microscope setup which is described in section 4. Stable NV^- centers were found in a concentration of 1 NV^- per 100 μm^2 (or 0.27 parts per trillion, ppt). After careful cleaning, we fix the sample on the three-axis nano-positioner in the UHV setup, see figure 1. The diamond was exposed to accelerated focused nitrogen ions of isotope $^{15}N_2^+$. Since each single nitrogen ion is trapped and identified prior to implantation, the dose can be controlled at a single ion level. A pattern of 5×5 was implanted with a distance of 2 μm between the single implantation spots by moving the sample with the nano-positioner. The dose κ can be adjusted freely and was varied from one to 20 ions per spot, see figure 3 for details. According to SRIM simulations the used 3 keV implantation energy per atomic ion corresponds to a penetration depth of 4.2 nm with an uncertainty of ± 2.2 nm and therefore the resulting NV centers can be considered as shallow [29].

The implanted sample was acid cleaned in a mixture of sulfuric, nitric and perchloric acid (ratio 1:1:1) which was heated to 130 °C for 2 h, in order to remove any dirt from the surface. Especially any graphitic layer which could be produced during the ion bombardment is removed by this treatment.

A successive annealing procedure under ultra-high vacuum was subsequently performed in order to activate NV centers. During this process, vacancies (empty lattice sites) that are created due to collisions during the implantation process, become mobile and pair with implanted nitrogen atoms forming stable

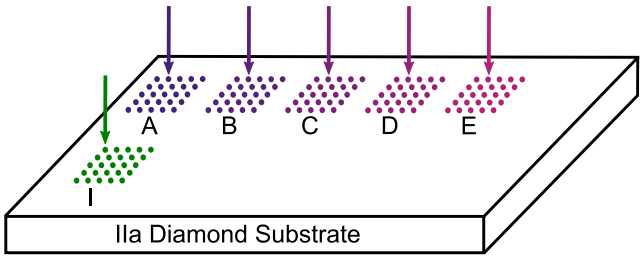

Figure 3. Implantation pattern with different ion quantities κ per spot which are separated by 2 μm. Region I (green) was implanted with $^{15}N_2^+$ and Ca^+, whereas the regions A–E (purple) were implanted with $^{15}N_2^+$ ions only. The different ion doses for the different regions are selected to be I: $\kappa_I = 20\ \frac{\text{ions}}{\text{spot}}$, A: $\kappa_A = 20\ \frac{\text{ions}}{\text{spot}}$, B: $\kappa_B = 10\ \frac{\text{ions}}{\text{spot}}$, C: $\kappa_C = 4\ \frac{\text{ions}}{\text{spot}}$, D: $\kappa_D = 2\ \frac{\text{ions}}{\text{spot}}$ and E: $\kappa_E = 1\ \frac{\text{ion}}{\text{spot}}$.

nitrogen-vacancy centers [30]. The temperature was set to 250 °C for 1 h to keep a high vacuum during the annealing process. Then, the temperature was ramped up to 900 °C and hold for another 2 h, with a vacuum of 10^{-7} mbar. Finally, the system was cooled down. Another acid boiling step was included to ensure the oxygen termination of the diamond surface, which is essential for the preservation of the NV^- charge state of shallow NVs [18, 31].

4. NV characterization

Confocal imaging was performed on a home-built confocal microscope consisting of a 518 nm diode laser, a movable micrometer stage, an oil immersion objective (NA = 1.4) and an avalanche photo diode. A lateral x–y-scan of the diamond sample can be seen in figure 4. Clearly visible are spots with high count rate (bright spots) coming from the NV center fluorescence to which the setup is optimized by an optical filtering system (excitation: 535/20BP, detection: 560LP). In total, six stable spots can be observed in region I (figure 4(a)), showing the typical fluorescence spectrum of NV centers, see figure 5. Some of them are present in the NV^0 charge state with no accessible electron spin and therefore cannot be used for electron spin resonance (ESR) measurements. The fluorescence spectrum of NV^0 shows a zero-phonon-line (ZPL) at 575 nm with a band to higher wavelengths. The ones which show a ZPL at 637 nm (as marked with red circles in figure 4(a)) are in the NV^- configuration and can be further investigated. These NV centers show fluorescence intensities which are typical for the presence of a single emitter. One of the key features of NV centers is that the fluorescence level itself depends on the state of its electron spin. Therefore the ESR transition of the NV center can be determined in an ODMR experiment. To this end, the NV is continuously irradiated with a green laser while a microwave with varying frequency is applied. In the absence of a magnetic field a zero field splitting of 2.87 GHz confirms the presence of an NV^- center. Furthermore, it is also possible to determine whether a center has formed due to the presence of nitrogen isotopes 14 or 15. To do this, the mutual effects described above must be minimized in order to obtain a resonance dip linewidth with which the hyperfine coupling to the nitrogen nucleus can be measured. A technique which offers this requirements is the pulsed ODMR technique where the microwave sweep is performed in a pulsed way inverting the electron spin states. Clearly visible is the separation of 3.1 MHz of the ODMR measurement in figure 6, which is related to presence of a ^{15}N nuclear spin.

A nitrogen 14 nuclear spin would be imprinted as a triplet in the ESR signal ($I = 1$), where the lines are separated by 2.2 MHz [32]. Only two of the found NVs show the hyperfine splitting of ^{15}N. Another one did show the triplet feature and the rest were present in the wrong charge state, so no ODMR signal was observed. The presence of ^{14}NV can be explained by the following. During the implantation of $^{15}N^+$ ions, collision to carbon atoms cannot be avoided even at low implantation energies, therefore vacancies are created when the ions penetrate into the diamond. The number of additional vacancies exceeds the number of ^{15}N ions. Also, if the Ca^+ is not blanked out, vacancies might be generated by its impact. The generated vacancies may recombine with natural ^{14}N atoms in the diamond substrate present in ppb concentration in electronic grade CVD diamond crystals [11]. Another explanation is that not solely ^{15}N ions were implanted but accidentally also ^{14}N ions, as the nitrogen reservoir was not immediately purged and refilled before implantation, see figure 2(a), and the Wien filter selectivity might not be sufficient. However, the origin of the ^{14}NV center cannot be clarified entirely.

The NV creation yield of our implantation is estimated by dividing the number of observed centers by the number of implanted nitrogen ions. In region I a total of 500 molecular nitrogen ions were implanted, with 6 NV centers visible we calculate an NV creation yield of 0.6% $\pm$ 0.2%. This is consistent with previous reports [33] at this low energies of implanted nitrogen ions. Note that a higher implantation dose

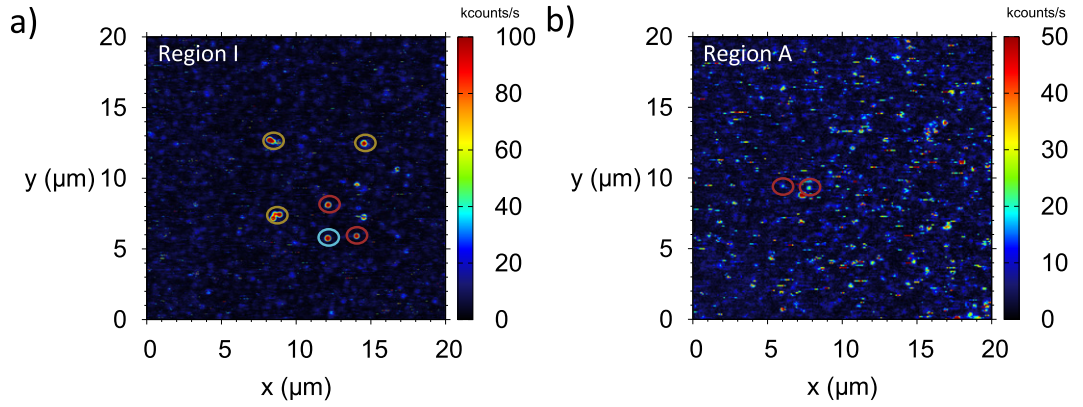

Figure 4. Confocal images of the implanted regions. (a) Region I: the bright spots correspond to NV centers present in the diamond. The presence of six NV centers on implanted sites, which fit to the implantation grid pattern of 2 μm distance, was confirmed by either optical fluorescence spectroscopy or electron spin resonance spectroscopy. Half of the confirmed centers were found to be in neutral charge state (yellow circled) and two with the implanted nitrogen isotope ^{15}N (red circled) and one with isotope ^{14}N (blue circled). (b) Region A: same analysis as in (a) reveals the presence of two NV centers of type nitrogen ^{15}N (red circled).

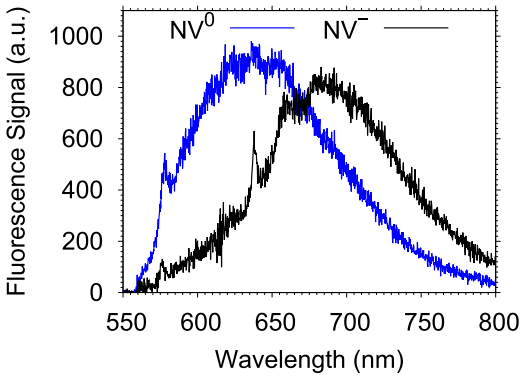

Figure 5. NV$^-$ (black) and NV^0 (blue) fluorescence spectra. The two different charge states are optically distinguishable since NV$^-$ shows a ZPL of 637 nm whereas the one for NV^0 lies at 575 nm.

of $\kappa = 200$ ions/spot did not result in NV center formation, which might be due to a locally not intact diamond lattice (graphitization).

The implantation attempts, without the co-implantation of Ca^+ (regions A–E), yield successful ^{15}NV center creation only in region A (highest dose), compare with figure 4(b). This suggests that the number of created vacancies, at very low doses, is limiting the creation yield. Note, that all NVs found there stem from $^{15}N^+$ implantation events. In order to assess the quality of the produced NV centers, Hahn echo measurements are carried out to determine the coherence time of the ^{15}NV centers in region I. This coherence time determines the maximum interaction time in potential sensing experiments and therefore plays a crucial role. The results of these measurements for the two $^{15}NV^-$ centers (i) and (ii) of region I can be found in figure 7. The values of 0.66 μs and 1.56 μs are by far not record breaking, but their determination for showing consistency of the used method, is more important than the absolute numbers. In fact, it is known that very shallow NV centers exhibit short coherence times [34, 35]. These short coherence times, most likely, stem from the proximity to the diamond surface, where a variety of paramagnetic fluctuations is present. It is possible to overcome these effects by using differently doped diamond as implantation material [36] or the recently reported so-called indirect overgrowth technique [37]. Another explanation for short coherence times might be the presence of carbon nuclear spins or the coupling to highly concentrated neutral-charged substitutional nitrogen (P1 center), in close proximity of the generated NV [38]. In our case, due to the tight implantation focus in combination with a low NV creation yield, indeed a high nitrogen atom concentration might be conjectured, as compared with non-focused implantation techniques at high impact energies.

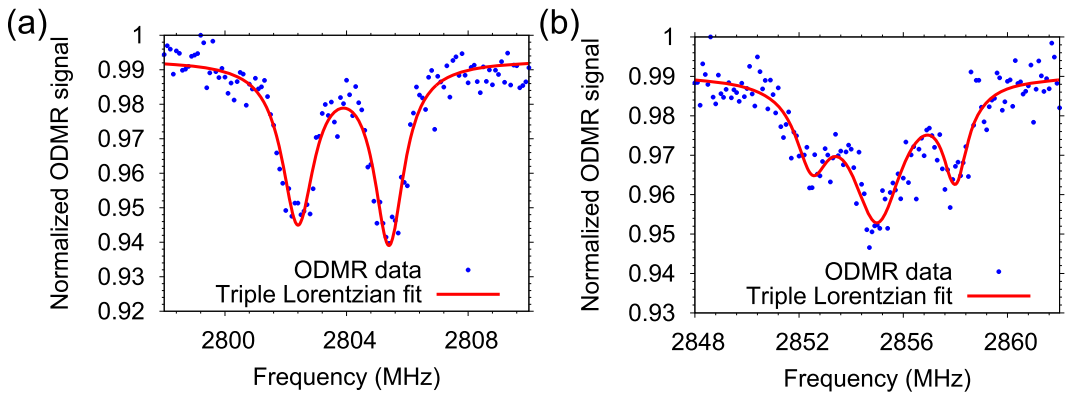

Figure 6. Pulsed ODMR spectra of the NV^- centers created by the deterministic implantation method. (a) Two lines, separated by 3.1 MHz correspond to the hyperfine coupling to ^{15}N nitrogen nucleus. This spectrum is proof that the implantation method is working as desired. The spectrum was recorded under the influence of a not specifically aligned, external magnetic field of approximately 23 G. (b) Hyperfine coupling of the NV's electronic spin to the nitrogen nuclear spin reveals the presence of a $^{14}NV^-$, since the characteristic three line structure becomes visible, where the lines are split by 2.2 MHz. The spectrum was recorded under the influence of an unaligned external magnetic field of approximately 5 G.

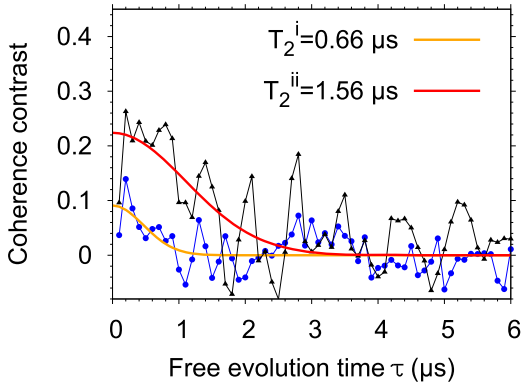

Figure 7. Hahn echo measurements performed on the successfully implanted $^{15}NV^-$ centers of region I. Coherence times of $T_2^{\mathrm{i}} = 0.66\ \mu s$ and $T_2^{\mathrm{ii}} = 1.56\ \mu s$ are measured for the NV^- centers (i) and (ii), respectively. The spectrum was recorded under the influence of an unaligned external magnetic field of approximately 70 G.

5. Perspectives

The demonstrated isotope-selective and maskless deterministic implantation results are encouraging for building a future quantum processor with coupled NV centers in diamond. Even though the yield in this work has been low, in the meantime pre-doping of diamond has been developed that allows for a yield up to 75% [17]. A pre-implantation with either phosphorous, oxygen or sulfur ions is followed by first annealing, thus preparing for the orders of magnitude improved yield upon the implantation of nitrogen and a second annealing step. Note, that already with a yield exceeding 50%, and in a rectangular lattice of qubits, a central NV center would have with 94% chance at least one next-neighbor NV qubit out of its four closest lattice qubits positions. If a lattice of qubits would be filled in such manner, it would be sufficiently populated for an effective perculation of entanglement. Improvements of both, the yield and the coherence properties are expected for shallow NVs if a higher annealing temperature of 1500 °C would be used. A second challenge is the selective qubit readout, especially for NV-qubit arrays with a grid dimension of about 10 to 20 nm. This is because optical readout schemes are limited to the Abbe diffraction limitation at about 0.2 μm, thus the individual NV^- or nuclear spin-qubits can only be distinguished in the frequency domain at cryogenic temperatures, but at the prize of spectral narrowing [12–14]. A recently demonstrated electrical readout of NV-qubit states [39] may be a potential solution, as a future architecture for NV-based quantum computing could use nano-wires on top of the diamond surface for selective readout of individual NV qubits at distances of about 20 nm, thus NVs sufficiently close to generate entanglement and execute fast gate operations. Group-four color centers (SiV, GeV, ZnV, PbV) show specific advantages, but their formation in diamond requires the creation of a split vacancy which is more difficult to produce. The implantation of adenine molecules, containing the required nuclei for color center generation and at the

same time those for a tailored nuclear spin environment, has been demonstrated recently [40]. Our results with trapped molecular ions as a source might be in future extended in this directions.

Acknowledgments

We thank Kilian Singer, Sam Dawkins, Luc Courturier and Sebastian Wolf for contributions at an earlier stage and acknowledge financial support by the Bundesministerium für Bildung und Forschung via Q.Link.X., the Volkswagen Stiftung and the Deutsche Forschungsgemeinschaft through the DIP program (Grant Schm 1049/7-1).

Data availability statement

The data that support the findings of this study are available upon reasonable request from the authors.

References

[1] Gruber A, Dräbenstedt A, Tietz C, Fleury L, Wrachtrup J and Von Borczyskowski C 1997 *Science* **276** 2012–4
[2] Müller C *et al* 2014 *Nat. Commun.* **5** 4703
[3] Meijer J, Burchard B, Domhan M, Wittmann C, Gaebel T, Popa I, Jelezko F and Wrachtrup J 2005 *Appl. Phys. Lett.* **87** 261909
[4] Riedrich-Möller J, Pezzagna S, Meijer J, Pauly C, Mücklich F, Markham M, Edmonds A M and Becher C 2015 *Appl. Phys. Lett.* **106** 221103
[5] Schröder T *et al* 2017 *Nat. Commun.* **8** 15376
[6] Hadden J P, Harrison J P, Stanley-Clarke A C, Marseglia L, Ho Y L D, Patton B R, O'Brien J L and Rarity J G 2010 *Appl. Phys. Lett.* **97** 241901
[7] Pezzagna S *et al* 2011 *Phys. Status Solidi* A **208** 2017–22
[8] Meijer J *et al* 2008 *Appl. Phys.* A **91** 567–71
[9] Neumann P *et al* 2008 *Science* **320** 1326–9
[10] Dolde F *et al* 2013 *Nat. Phys.* **9** 139–43
[11] Yamamoto T *et al* 2013 *Phys. Rev.* B **88** 201201
[12] Wu Y, Wang Y, Qin X, Rong X and Du J 2019 *NPJ Quantum Inf.* **5** 9
[13] Abobeih M H, Randall J, Bradley C E, Bartling H P, Bakker M A, Degen M J, Markham M, Twitchen D J and Taminiau T H 2019 *Nature* **576** 411–5
[14] Bradley C, Randall J, Abobeih M, Berrevoets R, Degen M, Bakker M, Markham M, Twitchen D and Taminiau T 2019 *Phys. Rev.* X **9** 031045
[15] Jakob A *et al* 2020 arXiv:2009.02892
[16] Jacob G, Groot-Berning K, Wolf S, Ulm S, Couturier L, Dawkins S T, Poschinger U G, Schmidt-Kaler F and Singer K 2016 *Phys. Rev. Lett.* **117** 043001
[17] Lühmann T, John R, Wunderlich R, Meijer J and Pezzagna S 2019 *Nat. Commun.* **10** 4956
[18] Hauf M *et al* 2011 *Phys. Rev.* B **83** 081304
[19] Lesik M *et al* 2016 *Phys. Status Solidi* A **213** 2788
[20] Schwartz J, Aloni S, Ogletree D F and Schenkel T 2012 *New J. Phys.* **14** 043024
[21] Groot-Berning K, Kornher T, Jacob G, Stopp F, Dawkins S T, Kolesov R, Wrachtrup J, Singer K and Schmidt-Kaler F 2019 *Phys. Rev. Lett.* **123** 106802
[22] Meijer J *et al* 2006 *Appl. Phys.* A **83** 321–7
[23] Schnitzler W, Linke N M, Fickler R, Meijer J, Schmidt-Kaler F and Singer K 2009 *Phys. Rev. Lett.* **102** 070501
[24] Izawa K, Ito K, Higaki H and Okamoto H 2010 *J. Phys. Soc. Japan* **79** 124502
[25] Groot-Berning K *et al* 2019 *Phys. Rev.* A **99** 023420
[26] Kaufmann H, Ruster T, Schmiegelow C, Luda M, Kaushal V, Schulz J, von Lindenfels D, Schmidt-Kaler F and Poschinger U 2017 *Phys. Rev.* A **95** 052319
[27] Jacob G, Groot-Berning K, Poschinger U G, Schmidt-Kaler F and Singer K 2016 *Proc. SPIE* **9900** 176–83
[28] Wübbena J B, Amairi S, Mandel O and Schmidt P O 2012 *Phys. Rev.* A **85** 043412
[29] Ziegler J 2012 The stopping and ranges of ions in matter www.srim.org
[30] Naydenov B *et al* 2010 *Appl. Phys. Lett.* **96** 163108
[31] Osterkamp C, Scharpf J, Pezzagna S, Meijer J, Diemant T, Behm R, Naydenov B and Jelezko F 2013 *Appl. Phys. Lett.* **103** 193118
[32] Rabeau J R *et al* 2006 *Appl. Phys. Lett.* **88** 023113
[33] Pezzagna S, Naydenov B, Jelezko F, Wrachtrup J and Meijer J 2010 *New J. Phys.* **12** 065017
[34] Staudacher T, Ziem F, Häussler L, Stöhr R, Steinert S, Reinhard F, Scharpf J, Denisenko A and Wrachtrup J 2012 *Appl. Phys. Lett.* **101** 212401
[35] Fukuda R *et al* 2018 *New J. Phys.* **20** 083029
[36] Fávaro de Oliveira F, Antonov D, Wang Y, Neumann P, Momenzadeh S A, Häußermann T, Pasquarelli A, Denisenko A and Wrachtrup J 2017 *Nat. Commun.* **8** 15409
[37] Findler C, Lang J, Osterkamp C, Nesládek M and Jelezko F 2020 *Sci. Rep.* **10** 22404
[38] Bauch E *et al* 2020 *Phys. Rev.* B **102** 134210
[39] Siyushev P *et al* 2019 *Science* **363** 728–31
[40] Haruyama M *et al* 2019 *Nat. Commun.* **10** 2664